Time-Resolved Stagnation Temperature Measurements in Hypersonic Flows Using Surface Junction Thermocouples

Byrenn Birch[1]

University of Southern Queensland, Toowoomba 4350, Australia

David Buttsworth[2]

University of Southern Queensland, Toowoomba 4350, Australia

Fabian Zander[3]

University of Southern Queensland, Toowoomba 4350, Australia

Abstract

Fast-response coaxial surface junction thermocouples have been used to measure time-resolved stagnation temperature of the Mach 6 flow produced by the University of Southern Queensland's hypersonic wind tunnel, TUSQ. The piston compression and the nozzle expansion of the test gas were found to be approximately isentropic for the first 65 ms of flow. Thereafter, the stagnation temperature reduces from $T_0 \approx 560\,\mathrm{K}$ due to the heat lost to the cold barrel, and this process can be modelled based on the measured barrel pressure history to simulate the stagnation temperature in TUSQ to within 2 % of the actual value for the first 150 ms of flow. By operating the thermocouples at the flow stagnation temperature, the fluctuations of the flow stagnation temperature were investigated. A $3 - 4\,\mathrm{kHz}$ narrowband stagnation temperature fluctuation appearing after $t \approx 65\,\mathrm{ms}$ was measured, and found to be correlated with the transition to turbulence of the flow in the barrel.

Keywords: stagnation temperature, hypersonic flow, heat flux, impulse response

1. Introduction

Stagnation temperature, and the fluctuation thereof, can have a significant impact in many hypersonic flow experiments [1, 2], but due to the impulsive loading and short test times in many facilities, these parameters can be difficult to measure. One such facility with short duration flows which commence and terminate rapidly is TUSQ, a hypersonic Ludwieg tube facility with free piston compression heating [3] which is located at the University of Southern Queensland. TUSQ produces quasi-steady cold flows of Mach 6 air for durations of approximately 200 ms which is a sufficiently long duration for the fundamental investigation of hypersonic mixing, aerodynamics, boundary layer flows, fluid-structure interactions, heat transfer and scramjet inlet starting.

The entropy disturbance mode (also referred to as total temperature fluctuations [4]) is temperature spottiness expressed as a percentage of the mean stagnation temperature, $\theta = \left(T'/\overline{T_0}\right) - \frac{\gamma-1}{\gamma}\left(T'/\overline{T_0}\right)\left(p'/\overline{p}\right)$ [1], and these disturbances are known to generate intense acoustic waves behind oblique shocks [5]. The interaction of oblique shocks and the freestream entropy waves can play an important role in boundary layer receptivity [6]. Fluctuations of stagnation temperature are not commonly measured in supersonic and hypersonic ground test facilities [4]. Hot wire anemometry

Email addresses: byrenn.birch@usq.edu.au (Byrenn Birch, david.buttsworth@usq.edu.au (David Buttsworth, fabian.zander@usq.edu.au (Fabian Zander

[1]Postdoctoral Researcher, School of Mechanical and Electrical Engineering

[2]Professor, School of Mechanical and Electrical Engineering

[3]Lecturer, School of Mechanical and Electrical Engineering

Nomenclature

$\dot{q}$	Heat flux	w	Shock speed
M	Mach number	x	Spatial coordinate normal to the surface
Nu	Nusselt number	***Greek symbols***	
Pr	Prandtl number	α	Thermal diffusivity
Re	Reynolds number	μ	Absolute viscosity
$\tilde{q}$	Time-invariant heat flux	ν	Thermal conductivity power law index
c	Specific heat	ω	Angular frequency
D	Diameter	ρ	Density
e	Thermal effusivity	σ	Standard deviation
f	Frequency	***Subscripts***	
G	Gain	0	Stagnation
h	Impulse response	1	Driven gas
h_c	Heat transfer coefficient	4	Driver gas
K	Stagnation point velocity gradient	5	Gas processed by the reflected shock
k	Thermal conductivity	∞	Freestream
P	Pressure	e	Edge of the boundary layer
R	Radius	i	Initial
S	Signal	p	Pre-flow
T	Temperature	pt	Pitot
t	Time	TC	Thermocouple
u	Velocity	w	Wall

(HWA) is the most common technique for the identification of total temperature fluctuations, however wires are prone to breakage [7], especially in flows with high dynamic pressures and/or impulsive flow starting/terminating properties. A cone probe fitted with atomic layer thermopile sensors have been used in a blowdown facility to measure heat flux fluctuations which, using complementary Pitot pressure and direct numerical simulations (DNS) to determine transfer functions, can be used to relate heat flux fluctuations to the freestream disturbances [8]. However, the proposed method is limited to very low Strouhal numbers for the incident disturbances meaning the gauge must be very small to perceive the post-shock entropy mode and therefore must approach a hot wire anemometer like system for high performance. Consequently, much of the literature for freestream flow characterisation using HWA is limited to continuous or intermittent flows in blowdown type facilities [2, 9, 10, 11] where the loading of the hot wire is not impulsive.

Previous measurements of the flow stagnation temperature in TUSQ were made using a thin wire thermocouple in an aspirating tube device [12]. These thermocouples responded to the initiation of flow within approximately 1 ms which was sufficient for resolving lower frequency temperature fluctuations and the results demonstrated a reduction in the flow stagnation temperature over the flow duration. However, improvements in the bandwidth of such stagnation temperature measurements would be needed to resolve fluctuations that arise due to turbulent mixing in the barrel.

Atomic layer thermopile (ALTP) sensors have a

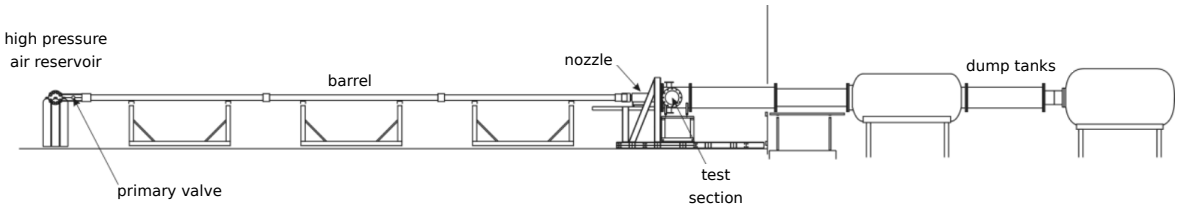

Figure 1: General arrangement of TUSQ.

time constant 2 to 3 times smaller than HWA which enables measurement of fluctuations up to 1 MHz and ALTP sensors have been used to measure fluctuations of heat flux on sharp cones [4, 9]. Measurements of freestream temperature fluctuations using ALTP sensors integrated on a wedge probe have been attempted by Wagner [13] who report a good signal-to-noise ratio (SNR), but did not present the data obtained because the sensitivity of ALTP sensors is subject to strong uncertainties.

Thin film and coaxial surface junction thermocouples have been used in cold-flow hypersonic facilities with mixed success [13, 14]. Because of the low SNR of these sensors, they are more suited to being positioned in the stagnation region than on the surface of inclined planes and cones, and it is the stagnation region configuration where successful measurements of heat flux have been made in cold flows.

A coaxial surface junction thermocouple is a simple construction consisting of an annular component and a pin which are separated by an electrically insulating layer such as epoxy [15] or an oxide coating [16]. The surface of the thermocouple is scratched to form junctions using different methods – commonly abrasive paper of different grit size or scalpel blades are used – with thinner surface junctions providing faster thermocouple response times [15]. The method of creating the surface junction is known to influence the effective thermophysical properties of the gauge [17], and therefore individual thermocouple calibration is preferred. Surface junction thermocouples are not normally designed to reach the flow temperature; these devices are primarily used to measure heat flux in transient applications and often referred to as 'heat flux gauges'.

If the heat transfer coefficient is known for a stagnation point heat flux gauge, the flow total temperature can be determined. The stagnation point heat transfer coefficient can be estimated analytically, or determined experimentally by operating the heat flux gauge over a range of surface temperatures [14], including thermocouple temperatures in excess of the flow stagnation temperature. The maximum operating temperature of epoxy-insulated surface junction thermocouples, which is limited by the epoxy, is well below the the stagnation temperature of TUSQ (nominally 560 K), and therefore this method of bonding and insulation is unsuitable for the preheated mode of operation for the measurement of the time-averaged and fluctuating components of stagnation temperature in TUSQ.

However, the surface junction thermocouples used in the present work are a relatively new matching-taper design relying on an oxide insulating layer and are suitable for operation at high temperatures. Previous experiments [18, 16] have demonstrated the utility of these rugged devices in expansion tunnel flows with durations of up to 200 µs with peak heat transfer rates in excess of $100\,\mathrm{MW\,m^{-2}}$. The present work investigates the application of these thermocouples in the low enthalpy, but long duration flows of TUSQ for the measurement of the time-averaged and fluctuating components of heat flux and flow stagnation temperature.

2. Facility and Test Condition

The University of Southern Queensland's Ludwieg tube with free piston compression heating (TUSQ, Fig. 1) is used to generate quasi-steady cold flows of hypersonic air for approximately 200 ms [3]. Prior to firing, the facility comprises three discrete volumes of gas: (1) the 350 L high pressure air reservoir; (2) the air in the Ludwieg tube (or barrel); and (3) the low pressure (< 1 kPa) region within the nozzle, test section and dump tanks. A 350 g piston is positioned in the barrel immediately downstream of the primary valve and a light Mylar diaphragm separates the barrel and nozzle inlet.

For the condition analysed herein (Table 1), the test gas initially residing in the barrel is at at-

mospheric pressure and ambient temperature. A run is initiated by opening the pneumatically actuated primary valve which causes the piston to be driven along the barrel by the flow of high pressure air from the reservoir, compressing the test gas. The pressure in the barrel is measured by a PCB113A03 piezoelectric pressure transducer positioned 225 mm upstream of the nozzle entrance (Fig. 2). The gradual opening of the primary valve nearly eliminates the occurrence of compression waves during the nominally isentropic compression process [19]. Compression continues until the pressure ruptures the diaphragm which then allows gas to leave the barrel and accelerate through the nozzle. The pressure in the reservoir is chosen so the volumetric flow rate into the barrel is approximately equal to the volumetric flow rate through the nozzle. This is known as a matched condition, where there is no net rise or fall in pressure over the run duration [20].

Table 1: Nominal TUSQ facility operating conditions.

Test Conditions	
Stagnation pressure	1 MPa
Stagnation temperature	575 K
Static pressure	670 Pa
Static temperature	71 K
Mach number	5.95
Unit Reynolds number	7.17×10^6 m^{-1}

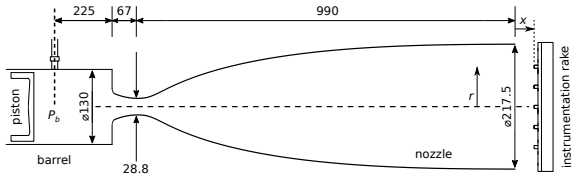

Figure 2: Schematic of Mach 6 nozzle and instrumentation rake position.

Five Type-E coaxial surface junction thermocouples were used for this research. These thermocouples were mounted in a bronze housing and interfaced with an existing instrumentation rake which held the thermocouples at the locations described in Table 2. These probe locations are all within the uniform core flow region that has been previously identified using Pitot pressure surveys [19].

Table 2: Positions of the thermocouples.

Thermocouple ID	x (mm)	r (mm)
TC2	50	40
TC4	50	20
TC6	50	0
TC10	50	20
TC13	50	40

3. Heat Flux Gauge

3.1. Design

Type-E (chromel-constantan) coaxial surface junction thermocouples were manufactured at USQ. The thermocouple design was a 3 mm long, 3.2 mm diameter chromel annulus with a 6/0 tapered hole, and a matching 4.5 mm long constantan pin as illustrated in Fig. 3. The constantan pin was oxidised in a temperature controlled furnace at 850 °C for 2 h, while the chromel annulus was not heat treated. The thin oxide layer on the constantan pin forms an electrically insulating layer between the two thermocouple legs when the thermocouple is assembled.

To assemble the thermocouple, the pin was pressed into the annulus with approximately 10 kg force. During the assembly process the oxide layer is prone to damage which can result in electrical shorting of the two thermocouple legs. The success rate was improved by introducing two drops of Resbond 907TS-Green thread sealant to the tapered hole of the annulus immediately prior to pressing the pin into the hole. When the assembly is pressed together the thread sealant is dispersed ahead of, around, and behind the pin. The increased assembly success rate was attributed to a combination of the thread sealant lubricating the components and the thread sealant immediately penetrating and filling any small scratches of the oxide layer.

Post assembly, thermocouple wires were spot welded to the rear of the thermocouple and the resistance of the thermocouple circuit was measured. By welding thermocouple wire, thermocouple material is maintained up to the thermocouple amplifier such that the thermocouple-copper junctions can be positioned in an isothermal environment. Using a flat solid surface, such as polycarbonate, as a backing material for the abrasive paper, the thermocouple face was then scratched using paper of increasing grit size until the resistance was in the order of 10 Ω or less, which indicated at least one

junction had been formed. Junctions formed with smaller grit sizes were likely to result in faster response thermocouples, however when it was clear a junction was unable to be created at a particular grit size, the next larger grit size was used. Should large particle sizes be required to form the junctions, the thermocouple response time could be improved by carefully polishing the surface with fine grit abrasive paper to reduce the depth of the junctions.

For use in the hypersonic flow of TUSQ, the thermocouples had to be mounted in a housing that interfaced with a probe support. An existing probe support [19] offered M5 × 0.8 threaded interfacing; this support was also used in the present work. To avoid the complexities of a non-uniform heat flux distribution on a hemisphere cylinder which is sometimes the preferred arrangement for heat flux probes [21], a flat faced geometry was selected. In this case, a constant heat flux is expected from the centreline of the body up to about $0.6R$ where R is the radius of the flat nosed body [22]. For a thermocouple diameter of $r = 1.6\,\text{mm}$, the minimum body radius of the flat nosed body was therefore 2.7 mm. However, for interfacing with the M5 × 0.8 rake geometry, a bronze housing with $R = 5\,\text{mm}$ was used. A flat-nosed body was also advantageous for the identification of the thermal effusivity of the thermocouple using the reflected shock calibration technique where a flat end wall is required.

Illustrated in Fig. 3, the 10 mm diameter flat faced probe is fitted with an enamelled nichrome resistance heating wire coil to preheat the thermocouple so that it can be operated at different initial temperatures which facilitates the experimental identification of the convective heat transfer coefficient h_c. The voltage output of the thermocouple was monitored throughout the heating process to ensure that the temperature of the thermocouple was stable prior to a run. A second probe head geometry of 10 mm diameter without the provision for the heating wire was also used.

3.2. Impulse Response Analysis

The unsteady conduction of heat within a solid body is described by a linear partial differential equation when the temperature gradients remain sufficiently small such that the thermal properties of the solid can be treated as constants. In a one-dimensional semi-infinite solid the unsteady conduction of heat is described by

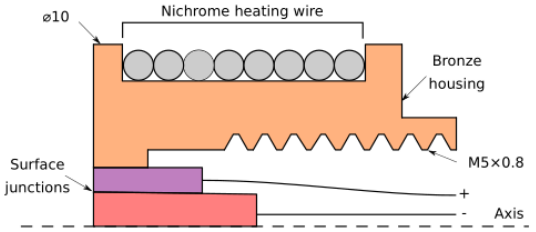

(a) Schematic of the heat flux gauge.

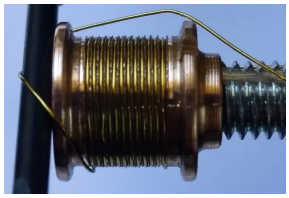

(b) Fitting of the heating wire.

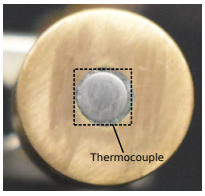

(c) Front view.

Figure 3: Design and images of the heat flux gauge.

$$\frac{\partial^2 T}{\partial x^2} = \frac{1}{\alpha}\frac{\partial T(x,t)}{\partial t} \tag{1}$$

where T is the temperature, x is the spatial coordinate normal to the surface, t is time, and α is the thermal diffusivity of the material.

The validity of the semi-infinite conduction assumption can be investigated by calculating the ratio of heat flux and temperature at a depth x to their wall values w, which for an isotropic semi-infinite solid, are

$$\frac{T_x}{T_w} = \exp\left(-\left(x^*\right)^2\right) - \sqrt{\pi}x^* \operatorname{erfc} x^* \tag{2}$$

and

$$\frac{\dot{q}_x}{\dot{q}_w} = \operatorname{erfc} x^* \tag{3}$$

where x^* is the dimensionless penetration depth $x^* = x/\sqrt{4\alpha t}$ [23]. For a test duration of 200 ms, $T_x/T_w = 1.5\%$ and $\dot{q}_x/\dot{q}_w = 3.3\%$ for the 3 mm long annulus; and $T_x/T_w = 0.1\%$ and $\dot{q}_x/\dot{q}_w = 0.4\%$ for the 4.5 mm long pin. The temperature change of the rear faces of the thermocouple components and the heat flow at these faces are a small fraction of the surface values. Therefore, for the thermocouple geometry and test time used, the thermocouples that form the measuring element of the heat flux gauge can be assumed semi-infinite. This conclusion is validated experimentally in Section 4.2 by investigating the measured heat flux after flow termination.

The heat flux gauge results were analysed using the impulse response method [24] which uses analytical models for one dimensional heat conduction within the gauge substrate to define suitable impulse response filters. In the case of a gauge operating on the principle of semi-infinite one dimensional heat conduction in an isotropic substrate, the value of thermal effusivity $\sqrt{\rho ck}$ of the substrate is required. A limitation of this analysis is that the thermocouple is assumed to be isotropic which is not the case. The thermal effusivity of the Type-E thermocouple materials are within one percent of each other, however the oxide and Resbond layers are also present and these additional materials potentially have an effect on the value of the thermal effusivity of the thermocouple. Additionally, the thermal contact conductance between the thermocouple materials cannot be considered by the analytical model. Nonetheless, a single value of thermal effusivity for the thermocouple can be determined experimentally via a suitable calibration technique.

3.3. Identification of Thermophysical Properties

The reflected shock calibration technique has been used to identify the thermal effusivity of surface junction thermocouples [17, 25]. To use the reflected shock tube calibration technique, the heat flux to the end wall containing the heat flux gauge must determined analytically and this process requires the knowledge of the properties of the gas in the shock tube.

The shock tube at USQ, shown schematically in Fig. 4, is capable of producing reflected shock temperatures in the order of 500 K. For the heat flux gauge calibration experiments, the shock tube was initially filled with ambient air from the surrounding laboratory environment. A light mylar diaphragm separated the driver and driven sections and the heat flux gauge was mounted on the centreline of the shock tube, flush with the end wall. Two pressure transducers, denoted PT1 and PT2 in Fig. 4, were mounted flush with the inside wall of the shock tube to identify the shock wave propagation along the shock tube. PT1 is located approximately 45 tube diameters downstream of the diaphragm station which is normally sufficient (5-40 tube diameters) for full shockwave formation at a constant velocity [26]. The pressure of the driver gas (air) was increased until the pressure differential at the diaphragm was great enough that the diaphragm ruptured.

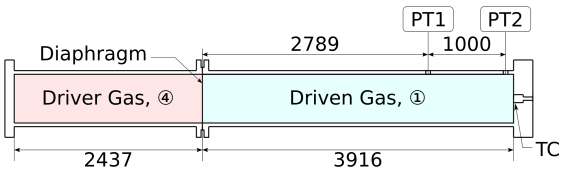

Figure 4: Shock tube geometry and instrumentation positions. The inside diameter of the shock tube is 63 mm.

Immediately following the diaphragm rupture, a shock wave is generated which propagates towards the end wall where the heat flux gauge is mounted (location shown in Fig. 4 as TC). The incident shock continues to propagate downstream until it reaches the end wall where it is reflected, and this reflection process provides the step input required for calculation of the thermal effusivity of the thermocouple. The thermocouple acts as a heat sink and, in theory, the surface of the thermocouple experiences an instantaneous change of temperature which, together with the properties of the gas which was processed by the reflected shock, is used to determine the thermal effusivity of the thermocouple e_{TC}.

The thermal effusivity of the gas at the reflected shock state, designated as state 5, is determined through normal shock relations for a calorically imperfect ideal gas based on initial conditions and the measured shock speed, w. A sudden pressure increase measured by PT1 and PT2 indicates the arrival of the shock wave. The pressure transducers are separated by a known distance (1000 mm) and the detection of the shock wave passing over the pressure transducers (indicated on Fig. 5) is used to determine the shock speed. The fast response of the thermocouple enabled an additional two measurements of shock speed to be obtained by measuring the time taken for the shock to travel the 1037 mm from PT1 to the thermocouple, and to pass from PT2 to the thermocouple. The three shock speed measurements determined from the pressure and temperature signals were within 2% of the mean value for each run, indicating a fully developed shock wave propagating at essentially constant velocity.

The temperature and pressure of state 1 are known a priori (the ambient laboratory environment), as is the temperature of state 4 (ambient temperature). Using the known properties and the measured shock speed, the properties behind the reflected shock can then be fully characterised.

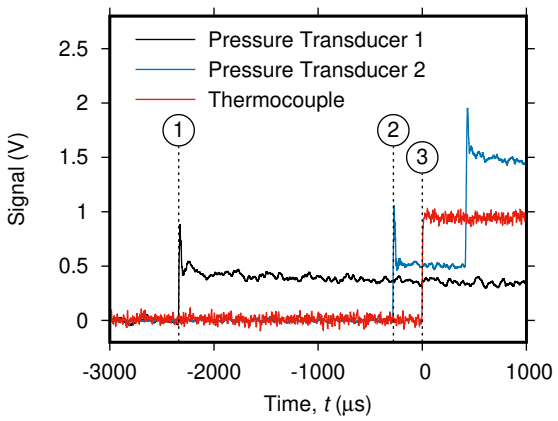

Figure 5: Raw data from a shock tube calibration of the thermocouple. The shock wave is detected by PT1 at 1, PT2 at 2, and by the heat flux gauge at 3.

The calibration shock speeds were from $458\,\mathrm{m\,s^{-1}}$ to $530\,\mathrm{m\,s^{-1}}$ and the temperatures behind the reflected shock were from 436 K to 520 K.

The heat flux to the end wall (w) from the gas behind a reflected shock (5) can be found using

$$\dot{q} = 1.13\sqrt{\frac{\rho_5 k_5 c_5}{2t}}T_5\left[\frac{1-\theta_w^{\nu}}{\nu} - \frac{1-\theta_w^{\nu+1}}{\nu+1}\right]^{\frac{1}{2}} \quad (4)$$

$$= \tilde{q}_w/\sqrt{t} \quad (5)$$

where $\theta_w = T_w/T_5$ and ν is the power law index for the thermal conductivity and $\tilde{q}$ is the time-invariant normalised heat flux quantity that depends only on the gas properties behind the reflected shock [27].

The surface temperature of the thermocouple that is flush with the end wall impulsively reaches a constant temperature when the shock is reflected as demonstrated in Fig. 5, and this temperature is determined using

$$T_{TC} = \frac{\tilde{q}\sqrt{\pi}}{e_{TC}} + T_{TC,i} \quad (6)$$

The raw voltage output of the thermocouple was converted to temperature using the standard ninth-order polynomial calibration [28] rather than the nominal $68\,\mu\mathrm{V\,^{\circ}C^{-1}}$ sensitivity of a Type-E thermocouple which is more than 10% greater than the actual thermocouple sensitivity at room temperature.

3.4. Thermophysical Properties of the Gauges

Five heat flux gauges were calibrated using the reflected shock calibration technique. For the reflected shock conditions used, the impulsive temperature rise of the thermocouple surface ranged from 0.282 K to 0.740 K. The thermal effusivity of the heat flux gauges was calculated using Eq. 6, and the results of 33 calibration shots are presented in Table 3. Resurfacing of the thermocouple junctions was often required before each calibration.

Table 3: Thermal effusivity of the thermocouples.

Gauge	Junction	$e_{TC} \pm \sigma$ $(\mathrm{J\,m^{-2}\,K^{-1}s^{-0.5}})$
TC2	1200 grit	$3965 \pm 10.8\,\%$
TC4	scalpel	$4172 \pm 4.9\,\%$
TC6	1200 grit	$4692 \pm 5.9\,\%$
TC10	2000 grit	$4667 \pm 3.7\,\%$
TC13	800 grit	$4005 \pm 3.6\,\%$
Mean	–	$4357 \pm 9.3\,\%$

The average thermal effusivity of the five heat flux gauges across the calibration tests was $4357\,\mathrm{J\,m^{-2}\,K^{-1}s^{-0.5}}$ which is significantly lower than the average thermal effusivity of two thermocouple materials ($8645\,\mathrm{J\,m^{-2}\,K^{-1}s^{-0.5}}$). This result was not unexpected; a significantly lower thermal effusivity for surface junction thermocouples of similar construction has been reported elsewhere [17, 25].

The reflected shock tube calibration also allows the identification of the response time of the heat flux gauges. TC2 had a higher variability of thermal effusivity than the other thermocouples. The rise time was defined as the time taken for the change of the thermocouple voltage to reach 63% $(1-1/e)$ of the step change. It is important to note that the amplitude of the step change of voltage is a function of the thermal effusivity of the thermocouple, not its rise time. Thermocouple TC6 had a rise time of approximately 3 µs, while the four other thermocouples consistently had rise times of less than 2 µs [29]. No trend relating the junction formation method to the thermocouple rise time was identified.

4. Data Analysis

4.1. Data Acquisition and Signal Conditioning

The data acquisition system at TUSQ, which uses 16-bit National Instruments PXI-6123 and PXIe-6124 multifunction I/O modules was used for this research. The sample rate for initial experiments was 2 MHz, but after analysis of these first results, the sample rate was revised to 50 kHz.

The thermocouple voltage signals were amplified using an in-house designed two-stage thermocouple amplifier with a bandwidth of 500 kHz. Stage 1 is a fixed DC gain of 100 (−3 dB at 500 kHz) and stage 2 an AC coupled stage (−3 dB at 3 Hz) with selectable gain as shown in Fig. 6. The amplifier was powered using a battery source so not to introduce noise from the mains power supply.

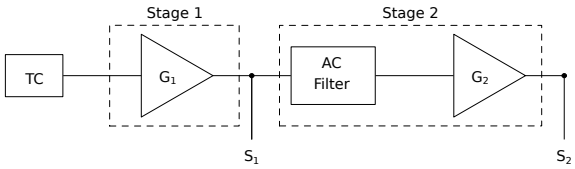

Figure 6: Two stage thermocouple amplifier schematic.

The maximum voltage signal that could be output by the amplifier is 5 V which for a Type-E thermocouple limits the maximum allowable DC amplifier gain to 200 if the thermocouples are pre-heated to the stagnation temperature of the Mach 6 flow. By using the AC coupled option for the second stage of the amplifier, the signal resolution can be improved significantly. However, the low-frequency components which are attenuated by the AC filter dominate the signal. By recording both a relatively low gain DC signal and a higher gain AC coupled signal it is possible to reconstruct the thermocouple signal with appropriately amplified higher frequency components.

The amplified thermocouple signal was found to contain a large amount of electromagnetic interference from a variety of sources (e.g. AM radio) which entered the circuit via the thermocouple junctions, and this interference was spread over a large number of narrow frequency bands. A 40 kHz lowpass filter was included, however significant baseline noise was still present, thus digital signal filtering was used.

Simple Butterworth filtering was found to be inadequate, and a stationary wavelet transform (SWT) filtering technique implemented. Both the amplifier output stages were filtered using a second-order level 6 symlet wavelet which, and an example of this filtering for a DC coupled signal is shown in Fig. 7. A thermocouple of 1 µs response time can be treated as having a 1 MHz bandwidth. When a signal from this thermocouple is processed by the second-order level 6 symlet wavelet, the effective bandwidth is reduced to 16 kHz.

A DC offset existed in the amplifier circuit, and

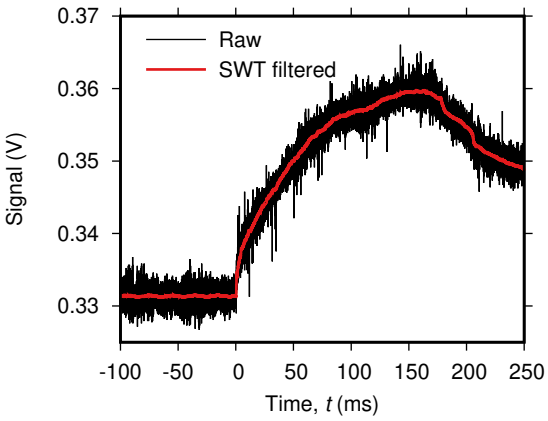

Figure 7: Conditioning of an amplified thermocouple (TC6, $T_i = 368.8$ K) signal for TUSQ Run 817 (Table 1) using SWT filtering.

therefore to correctly determine the electromotive force (emf) generated by the thermocouple, the DC offset introduced during the amplification stage had to be removed. The DC offset for S_1 was identified by performing a cold calibration at a known temperature prior to the preheating of the thermocouple. The emf of the thermocouple as measured from S_1 was found using

$$\mathrm{emf}_{S_1} = \frac{S_1}{G_1} - \frac{S_{1,cold}}{G_1} + \mathrm{emf}_{\mathrm{E}}(T_{cold}) \qquad (7)$$

where $S_{1,cold}$ is the signal from the cold reference and $\mathrm{emf}_{\mathrm{E}}(T_{cold})$ is the known emf of a Type-E thermocouple at $T = T_{cold}$.

The emf as measured from S_2 is

$$\mathrm{emf}_{S_2} = \frac{S_2}{G_1 + G_2} - \frac{\overline{S_{2,p}}}{G_1 + G_2} \qquad (8)$$

where subscript p indicates pre-flow data and overline indicates a mean value. The results of Eq. 7 and Eq. 8 are shown in Fig. 8 for a representative experiment illustrating the process for transformation of the AC coupled signal to a true DC level.

A correction signal, analogous to the portion of the signal attenuated by the AC filter, can be identified by first calculating $\mathrm{emf}_{S_1} - \mathrm{emf}_{S_2}$, and then low-pass filtering to remove the high frequency difference signal. A suitable digital low-pass filter cutoff frequency is high enough to reconstruct the mean shape and level of emf_{S_1} but low enough that the transformation process does not lose significant low frequency fluctuation content. Through an iterative process, a 50 Hz cutoff frequency was found to be suitable for this work.

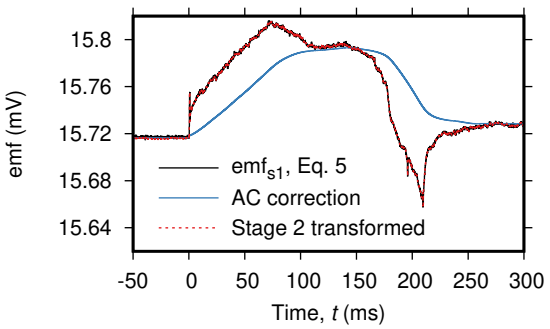

(a) DC coupled signals

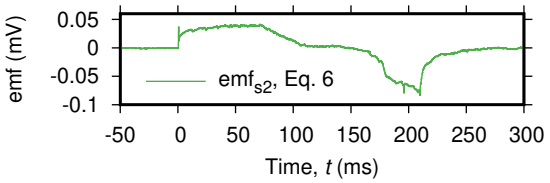

(b) AC coupled signal

Figure 8: Transformation of an AC coupled signal to a DC signal level. Data of TC4 obtained from Run 818.

An interesting feature to note from Fig. 8 is that, for about the first 60 ms of flow, the raw thermocouple data has identified the reflected expansion waves that reflect off the piston and propagate into the test flow. This demonstrates that the SWT filtering technique preserved the sharp changes of the raw thermocouple voltage and therefore retained a large amount of physical flow data.

4.2. Heat Flux

Following the reconstruction of the thermocouple signal, the thermocouple emf was used to determine the temperature of the thermocouple junctions. Three thermocouples were mounted in housings that were wrapped with nichrome heating wire and two were not fitted with any heating wire. Despite there being no heating control for two of the thermocouples, thermal conduction through the rake resulted in a moderate temperature rise when neighbouring thermocouples were heated.

The heat flux ($\dot{q}$) was calculated from the measured thermocouple temperature history (T) using the impulse response filtering technique [24] with the mean values of e_{TC} from Table 3. The change of the thermocouple temperature for three runs at different pre-heat temperatures is shown in Fig. 9a, and the heat flux for these data shown in Fig. 9b. Large non-repeatable spikes in the temperature data are evident in Fig. 9a. Similar effects were observed in earlier Pitot pressure surveys [19] and has been attributed to the effects of small particulates which contaminate the measurement of the flow, so are omitted from Fig. 9b.

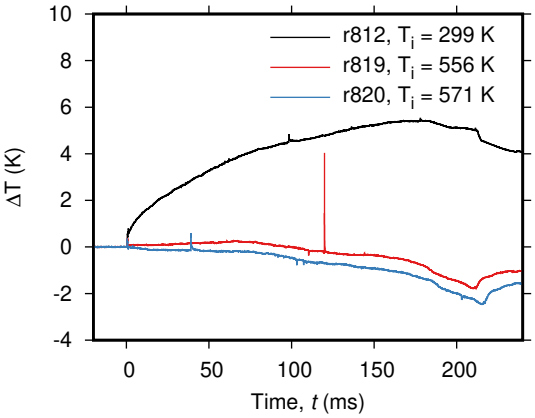

(a) Thermocouple temperature

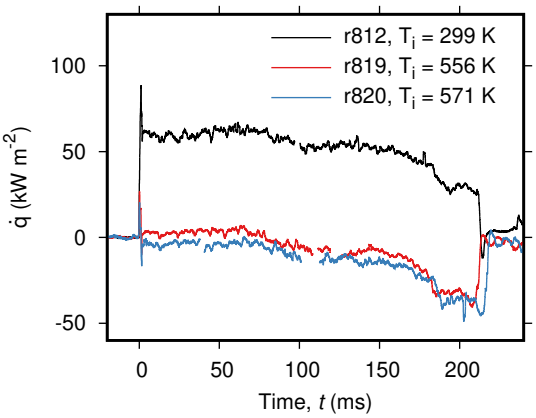

(b) Heat flux

Figure 9: Thermocouple temperature and the identified heat flux calculated using the method described by Oldfield [24] for three runs using TC10 which operated at three different temperatures.

The heat flux for the first several tens of milliseconds for Run 819 was slightly positive while for this time period the heat flux was slightly negative for Run 820. This indicates that, if the flow conditions in the two runs were identical, the stagnation temperature for the first 60 ms was bound between 556.2 K and 570.6 K. As shown in Fig. 9b, the measured heat flux immediately returns to zero upon flow termination at about $t = 210$ ms, indicating that the semi-infinite solid assumption is appropriate. After the initial return to $\dot{q} = 0\,\mathrm{kW\,m^{-2}}$ upon flow termination there are small oscillations of heat flux which trend away from zero. This is because the heat transfer gauge is subject to pres-

sure wave disturbances as the test section pressure equilibrates with the dump tank.

4.3. Identification of the Heat Transfer Coefficient and Stagnation Temperature

The transient heat flux ($\dot{q}$) identified by the surface junction thermocouples can be described by

$$\dot{q} = h_c \left(T_0 - T_w \right) \tag{9}$$

where h_c is the heat transfer coefficient, T_0 the stagnation temperature, and T_w the temperature of the thermocouple face. If the heat transfer coefficient of the thermocouple probe is known or can be approximated with reasonable accuracy, the flow total temperature can be estimated using single measurements of thermocouple temperature and transient heat flux.

An analytical model exists for estimating the heat transfer coefficient which requires knowledge of flow parameters. In the stagnation region of a flat nosed axisymmetric body in hypersonic flow, the heat transfer coefficient can be approximated analytically by

$$h_c = 0.763 \, \mathrm{Pr}_e^{-0.6} \sqrt{\rho_e \, \mu_e K} \times \left(\frac{\rho_w \, \mu_w}{\rho_e \, \mu_e} \right)^{0.1} c_{p,avg} \tag{10}$$

where Pr is the Prandtl number, ρ is density, μ is the absolute viscosity, K is the local velocity gradient, $c_{p,avg}$ is the average of the specific heats $c_{p,e}$ and $c_{p,w}$, and the subscripts e and w denote the conditions at the edge of the boundary layer and wall respectively [30]. The local velocity gradient K at the stagnation point in not known precisely but is approximated as $0.3u_\infty/D$ [30] so there is a some uncertainty in the analytical value of h_c.

Under the assumption of isentropic compression and expansion within the TUSQ facility with the freestream Mach number of 5.95, $h_c \approx 206 \, \mathrm{W \, m^{-2} \, K^{-1}}$ for a 10 mm diameter flat-faced probe operated at $T_i = 300 \, \mathrm{K}$. Given the unquantified uncertainties in the stagnation point velocity gradient a more reliable method for determining the heat transfer coefficient and flow stagnation temperature is desirable.

By operating nominally identical gauges at different temperatures for nominally identical runs, different transient heat fluxes are measured. The convective heat transfer coefficient is only a weak function of the surface temperature ($T_w^{0.0334}$) and flow total temperature ($T_0^{0.2028}$), and therefore h_c can be assumed constant to within the accuracy of the heat flux measurements as

$$T_{w,n} = -\frac{\dot{q}_n}{h_c} + T_{0,n} \tag{11}$$

where n is the $\mathrm{n^{th}}$ run and since $T_{w,n}$ and $\dot{q}_n$ are known and h_c assumed constant, with data from thermocouples at different temperatures, a linear regression analysis can be performed to determine h_c and T_0.

For each run, the thermocouple temperature and the heat flux data for window lengths 10 ms at multiple stages throughout the run were analysed using a linear regression. A sample of the data produced from this process is shown in Fig. 10 with the regression line for TC10 also included. For cold operation there was significant spread in the data which resulted in a poor linear regression, but the data does show a trend similar to the regression for TC10. This apparent co-linearity indicates that any changes in thermal effusivity at elevated operating temperatures was not significant.

The heat transfer coefficient tended to increase slightly with the run duration which is predicted by Eq. 10 as the Mach number decreases, but were always within 5% of the mean h_c for the gauge [19]. These changes were small and well within the uncertainty of heat transfer measurements, therefore a single mean heat transfer coefficient was deduced for each gauge. Thermocouple TC2 was found to electrically short to the probe housing in a heated mode of operation, while TC6 and TC13 were not fitted with heating wire. Therefore, h_c could only be experimentally identified as $h_c = 229 \, \mathrm{W \, m^{-2} \, K^{-1}}$ and $h_c = 232 \, \mathrm{W \, m^{-2} \, K^{-1}}$ for TC4 and TC10 respectively. Since the remaining probes were the same geometry as TC4 and TC10, a convective heat transfer coefficient of $h_c = 230 \, \mathrm{W \, m^{-2} \, K^{-1}}$ was assumed for these gauges. This is 12% more than predicted by Eq. 10, suggesting that the approximation (described as an educated guess by White [30]) of $K = 0.3u_\infty/D$ was reasonable, but that significant errors will arise if the analytical model was used. A zero heat flux case exists when the thermocouple operating temperature matches the flow stagnation temperature; this case is shown on Fig. 10 at $T_w = T_0 \approx 560 \, \mathrm{K}$.

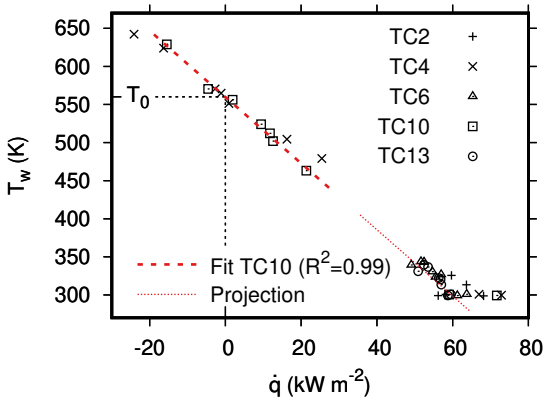

Figure 10: Identification of h_c using experimental data for $5\,\text{ms} \leq t \leq 15\,\text{ms}$.

5. Results

5.1. Temporally Resolved Stagnation Temperature

For each experiment, the temporally resolved stagnation temperature T_0 was calculated using

$$T_0 = \frac{\dot{q}}{h_c} + T_w \tag{12}$$

with h_c applied for each gauge defined from the method in Section 4.3

The stagnation temperature which was identified for each run was low-pass filtered at 1 kHz using a 256 point Blackman-Harris window. The 1 kHz bandwidth was sufficiently high to resolve relatively high frequency events, such as those associated with reflections of the expansion wave off the piston propagating into the test flow.

The stagnation temperature data at each position for every run was temporally aligned such that flow onset occurred at $t = 0\,\text{ms}$. This signal alignment enabled identification of the mean stagnation temperature across all TUSQ runs at every time step and each thermocouple. The mean level comparison is shown in Fig. 11 for $t \leq 30\,\text{ms}$.

For $t < 10\,\text{ms}$, the stagnation temperature calculated using data from thermocouples operated without preheating tended to exceed the value of the stagnation temperature calculated by isentropic compression of the test gas. This behaviour was not observed when using preheated thermocouples, and for $t > 10\,\text{ms}$ the heated and preheated thermocouples produce similar results. For $t < 10\,\text{ms}$, the preheated thermocouples (TC4, TC10) were found to resolve the flow stagnation temperature better than the cold thermocouples (TC6, TC13).

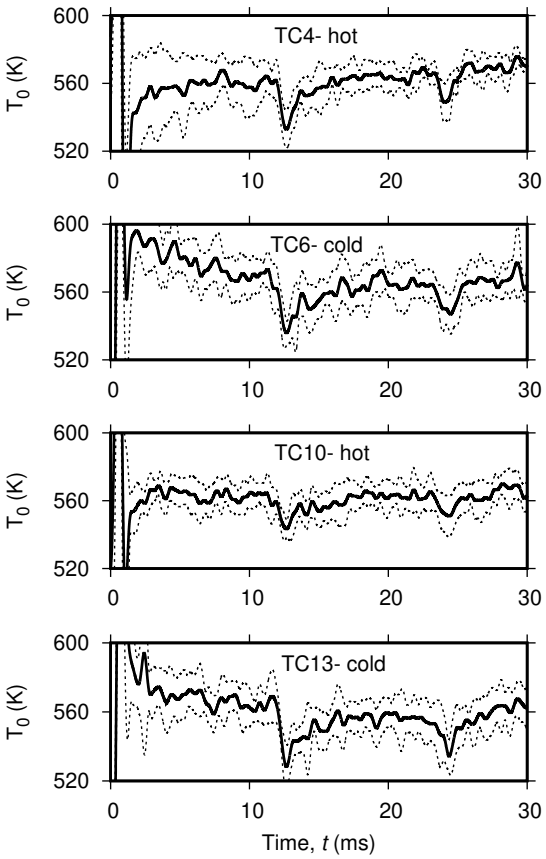

Figure 11: Comparison of flow stagnation temperature for $0 \leq t \leq 30\,\text{ms}$ measured by four thermocouples. Dashed lines indicate one standard deviation of stagnation temperature from the mean for all measurements using that thermocouple.

The initial overshoot behaviour of the cold thermocouples is the period of greatest variance between runs, but the standard deviation of stagnation temperature from 8 to 30 ms is consistent for cold and heated thermocouples. For this period of flow across all runs, the standard deviation of the stagnation temperature was 1.58 % for both TC4 and TC10, while the standard deviation of the cold thermocouples, TC6 and TC13, was 1.96 % and 1.97 % respectively. The lower ru $\dot{q}/h_c$ term of Eq. 12 and the uncertainties associated therewith smaller.

The stagnation temperature of the hypersonic flow as identified using $f_c = 1\,\text{kHz}$ and the data from TC10 is shown in Fig. 12, illustrating good run-to-run repeatability. The mean flow line terminates at the end of the run with the shortest flow duration (approximately 206 ms). The pre-flow

data ($t < 0$ ms) represents the initial temperature of the thermocouple and also shows the baseline noise level of the measurements, which varied between runs.

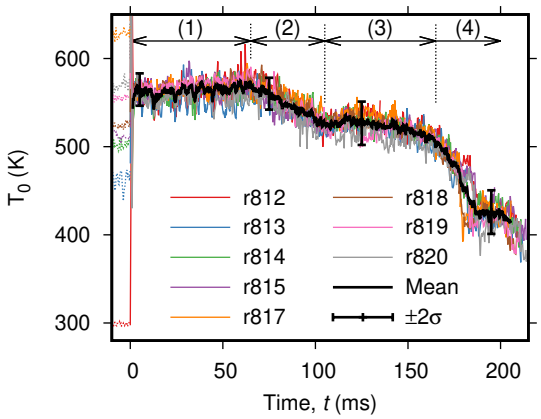

Figure 12: Stagnation temperature traces identified using TC10 over the full duration of the flow for $f < 1$ kHz. The time averaged line terminates at the end of the run with the shortest flow duration. Dashed lines indicate pre-flow data and represent the initial temperature of the thermocouple.

Using TC10, the average stagnation temperature for each run in the first 10 ms of flow is between the preheat temperatures for Run 819 (556.2 K) and Run 820 (570.6 K). This is consistent with the results presented in Fig. 9a where the thermocouple temperature increased by a small amount for Run 819 and dropped slightly during Run 820 for $0 < t < 10$ ms which corresponded to a slightly positive and slightly negative heat flux for Runs 819 and 820 respectively (Fig. 9b). Therefore, the flow stagnation temperature immediately following diaphragm rupture can be confidently stated as being in the range 556.2 to 570.6 K, which is just below the isentropic stagnation temperature (570 to 580 K).

An approximately constant stagnation temperature between diaphragm rupture and the arrival of the first wave reflected off the piston at approximately 12.5 ms was expected because the nozzle supply pressure remained constant during this period, and a constant stagnation temperature during this period of flow was confirmed experimentally.

Figure 12 shows that, for TC10, there were six runs where the initial probe temperature was $450\,\text{K} < T_{w,i} < 580\,\text{K}$ which resulted in $T_w \approx T_0$ for different periods of flow, and the regions where this is true are the periods of flow where stagnation temperature fluctuations can be analysed. Additionally, the stagnation temperature identified when $T_w \approx T_0$ are the periods of smallest measurement uncertainty as the effects of changes of effective thermocouple effusivity, and the uncertainty of the heat transfer coefficient are minimised.

As shown on Fig. 12, the stagnation temperature is approximately constant for the first 65 ms of flow (period 1), followed by a period of cooling by about 50 K over the next 40 ms (period 2). For $105 \lesssim t \lesssim 165$ ms the stagnation temperature is again approximately constant (period 3). When $t > 165$ ms (period 4) the rate of cooling increases until a sudden drop in stagnation temperature down to approximately 420 K. This sudden drop in stagnation temperature takes less than 2 ms and begins at a time $177 < t < 187$ ms, depending on the run.

To investigate if any of these changes in stagnation temperature can be attributed to events identified from the analysis of the stagnation pressure, a comparison of representative barrel and Pitot pressure traces and the mean stagnation temperature identified using each of the thermocouples is shown in Fig. 13. Since the barrel pressure measurement is spatially separated from the Pitot pressure and thermocouple measurements, a small time shift is applied to the barrel pressure signal to properly align the pressure and temperature signals. The annotations (i), (ii) and (iii) were identified from the barrel and Pitot pressure measurements, and these features are discussed in detail in [19]. The stagnation temperature is spatially uniform across the core flow, at least to the accuracy of transient heat flux measurements. The stagnation temperature in the vicinity of TC13 appears to be slightly cooler than that of the other probes for $40 < t < 80$ ms, however it is observed to agree well with measurements from the other locations for the remaining test time.

Stagnation temperature measurements were able to resolve the effects associated with the interaction of expansion waves and the piston (feature i, Fig. 13), with the first four wave reflections clearly visible on all of the mean traces. Later reflections are less evident on the mean traces because the temporal misalignment of these events becomes more significant as time increases.

Feature (ii), the reflected expansion wave that has travelled to the upstream end of the barrel returning to the nozzle inlet, occurs during a period of reducing stagnation temperature. However the start of cooling event (I) leads the arrival of (ii) by

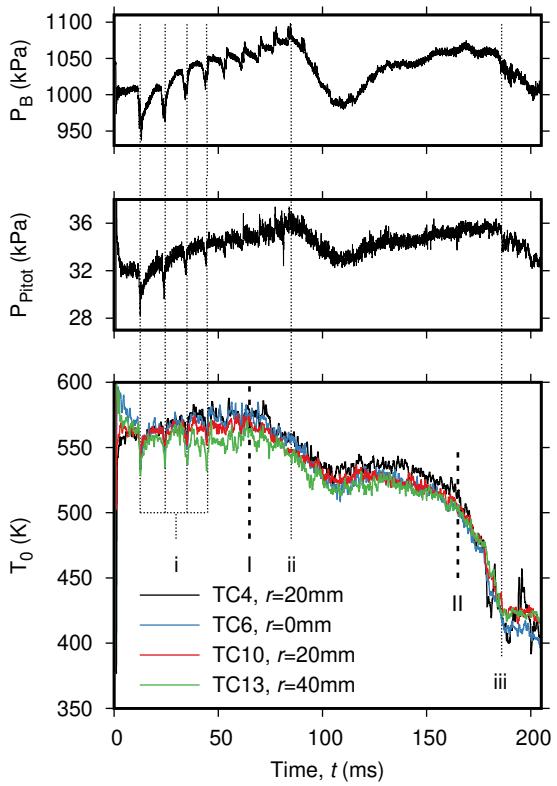

Figure 13: Barrel pressure, centreline Pitot pressure and the mean stagnation temperature, annotated with pressure events originating in the barrel. (i)- the first four reflected expansion waves off the piston; (ii)- the reflected expansion wave that has travelled to the upstream end of the barrel returning to the nozzle inlet; (iii)- reflected expansion wave (ii) returns to the nozzle inlet end of the barrel for the second time. Two changes in the stagnation temperature have been annotated: (I) the start of the first cooling event, and (II) the start of a second cooling event. Pressure data from Run 500 [19].

approximately 18 ms, and the rate of cooling after its arrival does not change. Therefore the cooling from 70 to 110 ms is not attributed to feature (ii).

Feature (iii), the reflected expansion wave (ii) returning to the nozzle inlet end of the barrel for the second time, occurs after the sudden reduction in stagnation temperature that begins at $t = 162$ ms, annotated (II) on Fig. 13. Therefore the sudden cooling event towards the end of hypersonic flow is not driven by the second reflected expansion wave (feature (iii)). Instead, the source of this sudden cooling and the lower stagnation temperature flow that occurs after the cooling is a result of cold vortical flow propagating ahead of the piston. Similar results were measured in TUSQ in an earlier study [12] and an unstable vortical structure is known to propagate ahead of the piston in similar piston driven facilities [31, 20].

Such vortical structures are known to adversely affect flow stagnation temperatures for the final 15 to 20% of the flow duration for barrels of large l/d ($\gtrapprox 100$) [31]. This vortex contains the tube boundary layer gas which has been scraped from the wall and therefore has a lower thermal energy content due to heat lost to the cold barrel walls.

5.2. Comparison to Simulation

A simulation tool to calculate the stagnation temperature in TUSQ based on the measured pressure in the barrel was developed by Widodo [12]. The simulation uses a thermodynamic model for the compression process based on the measured pressure history and engineering correlations for the heat loss from the test gas to the cold barrel walls during the compression and nozzle discharge processes. The heat transfer correlation based on a flat plate boundary layer was shown superior to the fully-developed pipe flow correlation [12].

A limitation of the original implementation is that the pressure in the barrel is assumed to be constant throughout the duration of flow discharge through the nozzle. This limitation was overcome in the present work by scaling the simulated stagnation temperature by the relative isentropic variations expected due to pressure-induced changes within the flow discharge period. In the original simulation code, laminar to turbulent transition of the flat plate boundary layer was assumed to occur in the range $0.2 \times 10^6 < \mathrm{Re} < 2 \times 10^6$. However, when used in this research, this range results in an early reduction of the stagnation temperature so the transition range was revised to $1 \times 10^6 < \mathrm{Re} < 2 \times 10^6$. The simulated stagnation temperature is compared to the experimentally measured stagnation temperature in Fig. 14.

With the time varying pressure effects now included in the simulation, the level of agreement between the flat plate model and experimental data is exceptional for the first 150 ms, remaining within 2 % of the experimental value. This error remains less than 5 % at $t = 170$ ms, and increases to approximately 20 % when the cold vortices ahead of the piston are discharged through the nozzle.

Three events that cause large changes of the stagnation temperature were identified (Fig. 14):

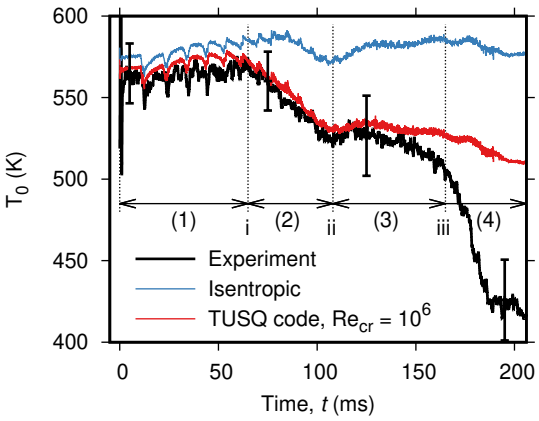

Figure 14: Comparison of the experimentally measured and simulated stagnation temperature for Run 819.

i) a reduction in stagnation temperature, the onset of which is associated with the barrel boundary layer transitioning according to the model;

ii) a point where the heat lost to the barrel can be modelled using a turbulent flat plate correlation; and

iii) a time when cold vortical flow propagating ahead of the piston is expelled through the nozzle.

The experimental data was compared to the temperature calculated from the measured barrel pressure using isentropic flow relations, and four periods of flow were be identified:

(1) for $t = 0\,\text{ms}$ to feature (i), a quasi-steady period of flow where T_0 is approximately 98 % of the isentropic stagnation temperature;

(2) from feature (i) to (ii), where T_0 reduces at a rate of approximately $1100\,\text{K}\,\text{s}^{-1}$;

(3) from feature (ii) to (iii), a second period of quasi-steady flow, albeit where T_0 reduces slowly; and

(4) from feature (iii) to the end of nozzle flow, where the cold vortices propagating ahead of the piston are expelled through the nozzle causing a large and sudden drop of stagnation temperature.

5.3. Fluctuations of Stagnation Temperature

The heat transfer coefficient for convective heat transfer to the stagnation point of an axisymmetric body in a high speed flow can be expressed in a non-dimensional form as:

$$\text{Nu} = 0.763\,\text{Pr}^{0.4}\,\text{Re}^{0.5}\,C^{0.1}\left(\frac{KD}{u_\infty}\right)^{0.5} \tag{13}$$

where Nu and Re are the Nusselt number and Reynolds number respectively, and both are referenced to the probe diameter, Pr the Prandtl number at the edge of the boundary layer, $C{=}\frac{\rho_w \mu_w}{\rho_e \mu_e}$ and $K{=}\frac{\mathrm{d}u_e}{\mathrm{d}x}$ is the local velocity gradient at the stagnation point.

In cases where Pitot pressure measurements are available, the heat transfer coefficient can be expressed as a function of Pitot pressure as:

$$h_c \propto \sqrt{P_{pt}} \underbrace{\left[\frac{k_e^{0.6}\,C^{0.1}}{\mu_e^{0.1}\,T_e^{0.25}}\right]}_{\text{(a)}} \underbrace{\left[M_\infty^{0.5}\left(\frac{T_\infty}{T_e}\right)^{0.25}\sqrt{\frac{KD}{u_\infty}}\right]}_{\text{(b)}} \tag{14}$$

where (a) terms represent the probe surface temperature and free stream total temperature effects, and (b) terms represent the Mach number effects [32]. The term $KD/u_\infty = 0.3$ is an approximation for M > 5 [30] for the case of a flat faced cylindrical probe. The sensitivity of h_c to the freestream Mach number in the present work can be determined by analysing Mach number dependent terms in Eq. 14 for the range $5.85 \leq \text{M} \leq 5.95$ [19]. It is found that the freestream Mach number term changes the heat transfer coefficient by $\lesssim$0.1 %. Therefore, the convective heat transfer coefficient is largely independent from the Mach number so the changes of the heat transfer coefficient resulting from the Mach number effect term can be neglected.

The relationship between the convective heat transfer coefficient and the probe surface and total temperature effects can be investigated by using the power law approximations for thermal conductivity and viscosity to show that

$$\left[\frac{k_e^{0.6}\,C^{0.1}}{\mu_e^{0.1}\,T_e^{0.25}}\right] \propto \frac{T_e^{0.2028}}{T_w^{0.0334}} \tag{15}$$

If the probe is operated at an essentially constant surface temperature, the heat transfer coefficient can be then expressed as

$$h_c = c\sqrt{P_{pt}}\,T_e^{0.2028} \tag{16}$$

where c is the constant of proportionality. The convective heat transfer coefficient can now be expressed in terms of time averaged (*e.g.* $\overline{h}_c$) and fluctuating components (*e.g.* h'_c) as

$$h_c = c\left(\overline{P}_{pt} + P'_{pt}\right)^{0.5}\left(\overline{T}_e + T'_e\right)^{0.2028} \tag{17}$$

which, via series expansion is

$$1 + \frac{h'_c}{\overline{h}_c} = \left(1 + 0.5\frac{P'_{pt}}{\overline{P}_{pt}}\right)\left(1 + 0.2028\frac{T'_e}{\overline{T}_e}\right) \tag{18}$$

when the second-order and higher terms are neglected. Since the product of $P'_{pt}/\overline{P}_{pt}$ and $T'_e/\overline{T}_e$ is a small contributor to Eq. 18, this term can be neglected and therefore,

$$\frac{h'_c}{\overline{h}_c} = 0.5\frac{P'_{pt}}{\overline{P}_{pt}} + 0.2028\frac{T'_e}{\overline{T}_e} \tag{19}$$

The heat flux can be expressed as time averaged and fluctuating components as

$$\dot{q} = \underbrace{\overline{h_c}\left(\overline{T_e} - \overline{T_w}\right)}_{\overline{\dot{q}}} + \underbrace{h'_c\left(\overline{T_e} - \overline{T_w}\right) + \overline{h}_c\left(T'_e - T'_w\right)}_{\dot{q}'} \tag{20}$$

and therefore,

$$\frac{\dot{q}'}{\overline{\dot{q}}} = \frac{h'_c}{\overline{h}_c} + \frac{T'_e - T'_w}{\overline{T_e} - \overline{T_w}} \tag{21}$$

Substituting Eq. 19 into Eq. 21, and considering that for a gauge operated at essentially constant temperature $T'_w \ll T'_e$,

$$\frac{\dot{q}'}{\overline{\dot{q}}} = \left(\frac{\overline{T_e}}{\overline{T_e} - \overline{T_w}} + 0.2028\right)\frac{T'_e}{\overline{T_e}} + 0.5\frac{P'_{pt}}{\overline{P}_{pt}} \tag{22}$$

The ratio $\frac{\overline{T_e}}{\overline{T_e} - \overline{T_w}}$ is at a minimum when evaluated for the case of an unheated thermocouple at the beginning of the run, where the stagnation temperature is at its maximum. In this case, $\frac{\overline{T_e}}{\overline{T_e} - \overline{T_w}} + 0.2028 \approx 2.25$, meaning the fluctuations in the measured heat flux are at least 4.5 times more sensitive to relative fluctuations in total temperature than to relative fluctuations in Pitot pressure. The heat flux is measured at the stagnation point, and since the stagnation temperature across a normal shock does not change, the flow temperature at the edge of the boundary layer T_e is therefore the flow stagnation temperature T_0. In a case where $T_w = 510\,\mathrm{K}$ and $T_0 = 560\,\mathrm{K}$, the relative fluctuations of heat flux are 22 times more sensitive to fluctuations in total temperature than to relative fluctuations in Pitot pressure. Therefore, it is desirable to operate a thermocouple as close to the flow stagnation temperature as possible to accurately determine stagnation temperature fluctuations. However when a thermocouple is operated at $T_w \approx T_0$, Eq. 22 is undefined since $\frac{\dot{q}'}{\overline{\dot{q}}} \to \infty$ and $\frac{\overline{T}_0}{\overline{T}_0 - \overline{T}_w} \to \infty$. Therefore, Eq. 22 is only suitable for specifying thermocouple operation when $T_w \neq T_0$.

Instead, for the case of $T_w = T_0$, the fluctuating component of heat flux is

$$\frac{\dot{q}'}{\overline{\dot{q}}} = \overline{h}_c\left(T'_0 - T'_w\right) \tag{23}$$

from Eq. 20. The magnitude of fluctuations of surface temperature for a surface junction thermocouple is related to the magnitude of heat flux fluctuation in the frequency domain by

$$\frac{|T'_w|}{|\dot{q}'|} = \left(\sqrt{\omega}\sqrt{\rho c k}\right)^{-1} \tag{24}$$

where ω is the angular frequency, $\omega = 2\pi f$, and $\sqrt{\rho c k}$ is the thermal effusivity of the thermocouple. Equation 24 can be written as

$$\frac{|T'_0|}{|T'_w|} = \overline{h}_c^{-1}\sqrt{\omega}\sqrt{\rho c k} + 1 \tag{25}$$

by using Eq. 23. Substituting $\overline{h}_c = 230\,\mathrm{W\,m^{-2}}$ and $\sqrt{\rho c k} = 4350\,\mathrm{J\,m^{-2}\,K^{-1}s^{-0.5}}$, Eq. 25 indicates the fluctuations in stagnation temperature are more significant than those of wall temperature by a factor of 100 at 4 Hz, and this ratio increases with increasing frequency. Thus, when T'_w is neglected relative to T'_0, from Eq. 23

$$T'_0 = \frac{\dot{q}'}{\overline{h}_c} \tag{26}$$

which is in a form that can be used to identify fluctuations of stagnation temperature when $T_w \approx T_0$.

Numerous regions of data were identified where the thermocouples were operated at approximately the stagnation temperature of the flow. To get the best estimates of stagnation temperature fluctuations, only regions where $T_0 = T_w \pm 15\,\mathrm{K}$ temperature were investigated. Due to the high baseline noise level in the measured thermocouple signal [29], the stagnation temperature fluctuation data was filtered using a Blackman-Harris window function with an effective low-pass filter cutoff frequency

of 3 kHz. The data was then high-pass filtered at 4 Hz to isolate the fluctuations of stagnation temperature.

Four periods of flow where $T_0 = T_w \pm 15\,\mathrm{K}$ are shown in Fig. 15, with these data belonging to periods 1 to 3 of Fig. 12. Fig. 15a shows the stagnation temperature fluctuations during period 1. During this period of flow the stagnation temperature fluctuations caused by the first two reflected expansion waves off the piston are visible at $t \approx 12.5$ ms and $t \approx 24.5$ ms.

The flow cooling experienced during period 2 is well represented by a laminar-turbulent flat plate transition, and the fluctuations of stagnation temperature during this period are shown in Fig. 15b. No reflected expansion waves are immediately evident, but the fluctuations of stagnation temperature exhibit a strong degree of periodicity with a period of approximately 250 µs.

Fig. 15c shows a segment of flow period 3 where the mean stagnation temperature is nominally constant and the heat transfer to the walls of the barrel is in agreement with the turbulent flat plate model. There appears to be some fluctuations with a period of approximately 500 µs. A later segment of flow period 3 is shown in Fig. 15d where a strong periodicity is evident.

The root-mean-square stagnation temperature fluctuations were 8.5 K, 10.7 K, 11.9 K, and 12.6 K for Fig. 15a to Fig. 15d respectively. However the baseline RMS noise level was in the order of 5 K with the signal-to-noise ratio ranging from 1.3 to 2.4 depending on the run. Therefore, the amplitude of the stagnation temperature fluctuations identified must be viewed with some caution.

Periodicity was identified in Fig. 7.18, and these fluctuations can be investigated using the power spectral density method. For this analysis only the relative magnitude of stagnation temperature fluctuations was of interest, and therefore to achieve the highest frequency resolution the 1 kHz low-pass filter was not implemented.

The baseline noise level was identified using a representative segment of data from prior to the flow onset. For frequencies above 5 kHz, the magnitude of stagnation temperature fluctuations was not sufficiently above the baseline noise level, and therefore the power spectral density (PSD) estimates shown in Fig. 16 are in the 0 – 5 kHz frequency band only.

No strong narrowband spectral content was identified in Fig. 16a, which is consistent with the Pitot

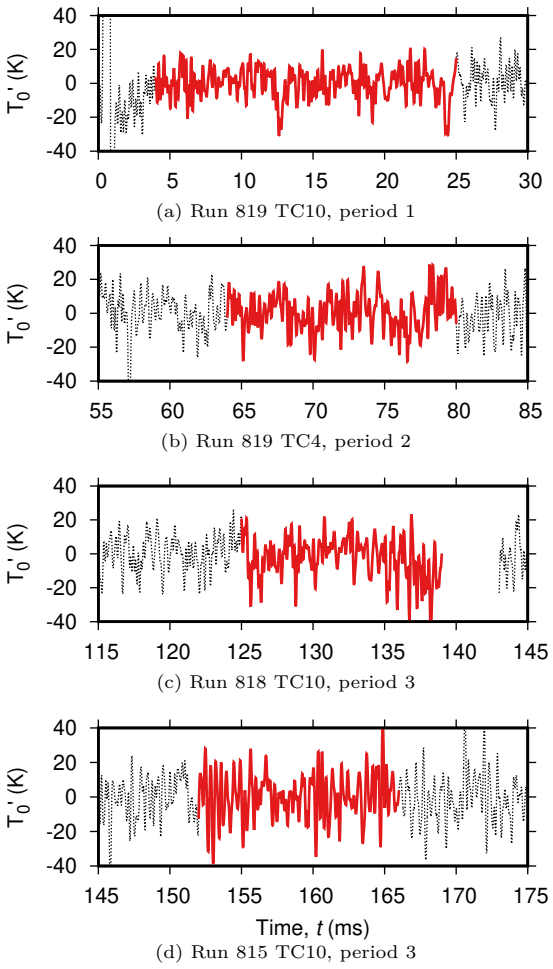

(a) Run 819 TC10, period 1

(b) Run 819 TC4, period 2

(c) Run 818 TC10, period 3

(d) Run 815 TC10, period 3

Figure 15: Stagnation temperature fluctuations during four 30 ms periods of flow where $T_w = T_0 \pm 15\,\mathrm{K}$ and $4\,\mathrm{Hz} \leq f \leq 3\,\mathrm{kHz}$. Dashed lines indicate data outside this window.

pressure fluctuations for the same time period [19]. Figure 7.20b exhibits a very strong spectral feature at 3.5 – 4 kHz. This feature was previously identified via a Pitot pressure survey and it was speculated to be approximately consistent with the return of the reflected expansion wave [19], shown as (ii) on Fig. 13. However, the start of this feature led the arrival of this reflected expansion wave by approximately 10 ms to 20 ms. The high amplitude 3.5 – 4 kHz spectral content is not evident in Fig. 16c, but is visible again in Fig. 16d.

The onset of the 3.5 – 4 kHz spectral content was analysed using PSD estimates of 20 ms periods of flow. This spectral content was not present before $t = 70$ ms, however when windowed to the 60 ms to 80 ms period of flow, a peak at 3.5 – 4 kHz was

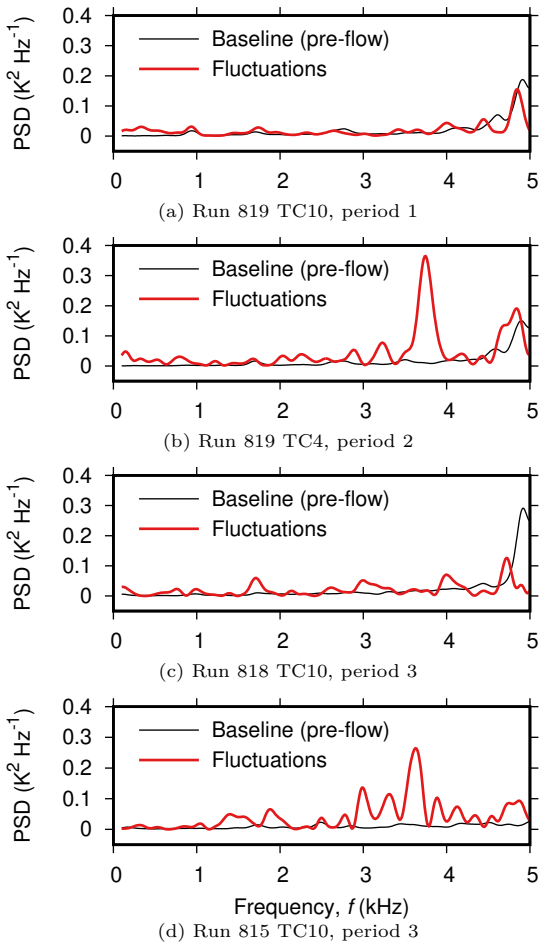

(a) Run 819 TC10, period 1

(b) Run 819 TC4, period 2

(c) Run 818 TC10, period 3

(d) Run 815 TC10, period 3

Figure 16: PSD estimates of the stagnation temperature fluctuations for the data presented in Fig. 15.

clearly visible. This suggests the onset of the 3.5 – 4 kHz spectral content occurs at 70 ms to 80 ms, and it is at about this time the heat transfer from the test gas in the barrel to the cold barrel walls was found to agree with flat plate transition from laminar to turbulent flow (Fig. 14). Therefore, the 3.5 – 4 kHz fluctuations of temperature and pressure that are present in the test flow for $t \gtrsim 70$ ms could be caused by the transition of the boundary layer of the test gas in the barrel from laminar to turbulent, not the reflected expansion wave as previously speculated [19].

As the present analysis cannot be used to infer the pre-shock (freestream) disturbance environment, the results are left as stagnation temperature fluctuations and not decomposed to the acoustic, entropy and vorticity mode. Further experimental work, likely via alternative intrusive or optical methods, is required to confirm if the 3.5 – 4 kHz disturbances are the result of transition of the boundary layer of the test gas in the barrel from laminar to turbulent.

The cooling effects that are caused by the piston compression process of the nozzle supply gas, and the fluctuations of total temperature which appear to also originate in the barrel, may also be present in other piston driven facilities or other facilities where heat transfer between the test gas and pipework can be significant. However, as there are a range of fundamentally different types of test facilities, strong conclusions about other facilities cannot be made. Instead, individual facility operators should investigate the stagnation temperature, and the fluctuations thereof, produced in their facility. Spurious peaks of unknown origin have been reported at 9.4 kHz at a Mach 10 condition and 40 kHz at a Mach 14 condition in the AEDC9 facility [33, 34], which could potentially be related to thermal disturbances in the nozzle supply region.

6. Conclusion

In this research, coaxial surface junction thermocouples with an oxide-insulated matching taper construction were used as transient heat flux gauges within blunt, cylindrical probes for the measurement of the flow stagnation temperature in a low enthalpy hypersonic wind tunnel with a flow duration of around 200 ms. The surface junction thermocouple construction allowed the gauges to be electrically heated to temperatures well above what is possible with the common epoxy insulating and bonding methods for construction. By operating these gauges at elevated temperatures, it was possible to measure the convective heat transfer coefficient for the probe arrangement.

The time averaged stagnation temperature of the flow produced by the Mach 6 nozzle of TUSQ was determined from measurements of the stagnation point heat flux. The experimental data was compared to the temperature calculated from the measured barrel pressure on the assumption of isentropic conditions, and four periods of flow were identified:

(1) for $t < 65$ ms where T_0 is approximately the isentropic stagnation temperature;

(2) for 65 ms $< t <$ 105 ms where T_0 reduces at a rate of approximately 1100 K s^{-1};

(3) for 105 ms $< t <$ 165 ms which is a period of nominally constant stagnation temperature; and

(4) for $t >$ 165 ms where the cold vortices that propagate ahead of the piston are expelled through the nozzle, resulting in a large sudden reduction of stagnation temperature.

The measured stagnation temperature was also compared to thermodynamic simulations based on the measured pressure history and empirical correlations for the barrel heat transfer. The simulated results are within 2% of the experimental data for $t = 0 - 150$ ms, increasing to 5% at $t = 170$ ms. For $t > 170$ ms, cold vortices that propagate ahead of the piston which are not modelled in the simulation increase the error of the simulation to 20%.

Root-mean-square stagnation temperature fluctuations were evaluated for $f = 4$ Hz – 5 kHz. RMS fluctuations of stagnation temperature, $\langle T_0' \rangle / T_0$, were observed to increase throughout the flow period, from approximately 1.5% at the start of a run to 2.4% at the end of a run. However, because there was a large amount of scatter (approximately ±0.5%) in the stagnation temperature fluctuation results, there remains significant uncertainty in these magnitudes. The onset of the 3 – 4 kHz disturbance was consistent with the onset identified by the Pitot pressure fluctuations reported elsewhere and appears to be initiated by flow transition in the barrel.

Surface junction thermocouples are frequently regarded as relatively low SNR devices that are not well suited to measurements in low enthalpy hypersonic flows. The results reported herein have conclusively demonstrated the capability to measure transient heat flux in one such flow with stagnation point heat flux values on the order of 10 kW m^{-2}, and the measurement of the wind tunnel stagnation temperature which varies over the 200 ms duration of the flow.

7. Acknowledgement

Byrenn Birch was supported by an Australian Government Research Training (RTP) Scholarship. Mr. Nathan Stern is thanked for the machining of the thermocouple components.

References

[1] L. S. Kovásznay, Turbulence in Supersonic Flow, Journal of the Aeronautical Sciences (Institute of the Aeronautical Sciences) 20 (10) (1953) 657–674. doi:10.2514/8.2793.

[2] D. Masutti, E. Spinosa, O. Chazot, M. Carbonaro, Disturbance Level Characterization of a Hypersonic Blowdown Facility, AIAA Journal 50 (12) (2012) 2720–2730. doi:10.2514/1.j051502.

[3] D. R. Buttsworth, Ludwieg Tunnel Facility with Free Piston Compression Heating for Supersonic and Hypersonic Testing, in: Proceedings of the 9th Australian Space Science Conference, National Space Society of Australia Ltd., 2010, pp. 153–162.

[4] D. Heitmann, T. Röediger, C. Kähler, H. Knauss, R. Radespiel, E. Krämer, Disturbance-Level and Transition Measurements in a Conical Boundary Layer at Mach 6, in: 6th AIAA Aerodynamic Measurement Technology and Ground Testing Conference, Vol. 3951, American Institute of Aeronautics and Astronautics, 2008. doi:10.2514/6.2008-3951.

[5] J. F. McKenzie, K. O. Westphal, Interaction of Linear Waves with Oblique Shock Waves, Physics of Fluids 11 (11) (1968) 2350. doi:10.1063/1.1691825.

[6] Y. Ma, X. Zhong, Receptivity of a Supersonic Boundary Layer Over a Flat Plate. Part 3. Effects of Different Types of Free-Stream Disturbances, Journal of Fluid Mechanics 532 (2005) 63–109. doi:10.1017/s0022112005003836.

[7] N. Parziale, J. Shepherd, H. Hornung, Free-Stream Density Perturbations in a Reflected-Shock Tunnel, Experiments in Fluids 55 (2) (2014) 1662. doi:10.1007/s00348-014-1665-0.

[8] T. Schilden, W. Schröder, S. R. C. Ali, A.-M. Schreyer, J. Wu, R. Radespiel, Analysis of Acoustic and Entropy Disturbances in a Hypersonic Wind Tunnel, Physics of Fluids 28 (5) (2016) 056104. doi:10.1063/1.4948435.

[9] S. R. C. Ali, J. Wu, R. Radespiel, T. Schilden, W. Schroeder, High-Frequency Measurements of Acoustic and Entropy Disturbances in a Hypersonic Wind Tunnel, in: 44th AIAA Fluid Dynamics Conference, American Institute of Aeronautics and Astronautics, 2014. doi:10.2514/6.2014-2644.

[10] A. E. Blanchard, J. T. Lachowicz, S. P. Wilkinson, NASA Langley Mach 6 Quiet Wind-Tunnel Performance, AIAA journal 35 (1) (1997) 23–28. doi:10.2514/2.82.

[11] J. Laufer, Aerodynamic Noise in Supersonic Wind Tunnels, Journal of Aerospace Sciences 28 (9) (1961) 685–692. doi:10.2514/8.9150.

[12] A. Widodo, D. Buttsworth, Stagnation Temperature in a Cold Hypersonic Flow Produced by a Light Free Piston Compression Facility, Experiments in Fluids 54 (4) (2013). doi:10.1007/s00348-013-1486-6.

[13] A. Wagner, E. Schülein, R. Petervari, K. Hannemann, S. R. C. Ali, A. Cerminara, N. D. Sandham, Combined Free-Stream Disturbance Measurements and Receptivity Studies in Hypersonic Wind Tunnels by Means of a Slender Wedge Probe and Direct Numerical Simulation, Journal of Fluid Mechanics 842 (mar 2018). doi:10.1017/jfm.2018.132.

[14] D. R. Buttsworth, T. V. Jones, High Bandwidth Stagnation Temperature Measurements in a Mach 6 Gun Tunnel Flow, Experimental Thermal and Fluid Science 27 (2) (2003) 177–186. doi:10.1016/s0894-1777(02)00281-9.

[15] S. Sanderson, B. Sturtevant, Transient Heat Flux Measurement Using a Surface Junction Thermocouple, Re-

view of Scientific Instruments 73 (7) (2002) 2781–2787. doi:10.1063/1.1484255.

[16] C. M. James, B. J. C. Birch, D. R. Smith, T. G. Cullen, T. Millard, S. Vella, Y. Liu, R. G. Morgan, N. Stern, D. R. Buttsworth, Testing of Ultra Fast Response, Durable Co-axial Thermocouples for High Enthalpy Impulse Facilities, in: 2019 AIAA Aviation and Aeronautics Forum and Exposition, American Institute of Aeronautics and Astronautics, 2019. doi:10.2514/6.2019-3007.

[17] D. R. Buttsworth, Assessment of Effective Thermal Product of Surface Junction Thermocouples on Millisecond and Microsecond Time Scales 25 (6) (2001) 409–420. doi:10.1016/s0894-1777(01)00093-0.

[18] R. T. P. Geraets, M. McGilvray, L. J. Doherty, R. G. Morgan, C. M. James, D. R. Buttsworth, Development of a Fast-Response Diamond Calorimeter Heat Transfer Gauge, Journal of Thermophysics and Heat Transfer 34 (1) (2020) 193–202. doi:10.2514/1.t5688.

[19] B. Birch, D. Buttsworth, R. Choudhury, N. Stern, Characterization of a Ludwieg Tube with Free Piston Compression Heating in Mach 6 Configuration, in: 22nd AIAA International Space Planes and Hypersonics Systems and Technologies Conference, American Institute of Aeronautics and Astronautics, 2018. doi:10.2514/6.2018-5266.

[20] T. Jones, D. Schultz, A. Hendley, On the Flow in an Isentropic Light Piston Tunnel, Tech. rep., Aeronautical Research Council, Reports and Memoranda, R & M No. 3731 (1973).

[21] V. Menezes, S. Bhat, A Coaxial Thermocouple for Shock Tunnel Applications, Review of Scientific Instruments 81 (10) (2010) 104905. doi:10.1063/1.3494605.

[22] N. Kemp, P. Rose, R. Detra, Laminar Heat Transfer Around Blunt Bodies in Dissociated Air, Journal of the Aerospace Sciences 26 (7) (1959) 421–430. doi:10.2514/8.8128.

[23] D. L. Schultz, T. V. Jones, Heat Transfer Measurements in Short-Druation Hypersonic Facilities, Tech. Rep. AGARD-AG-165, Advisory Group for Aerospace Research and Development (1973).

[24] M. L. G. Oldfield, Impulse Response Processing of Transient Heat Transfer Gauge Signals, Journal of Turbomachinery 130 (2) (2008) 021023. doi:10.1115/1.2752188.

[25] E. Marineau, H. Hornung, Modeling and Calibration of Fast-Response Coaxial Heat Flux Gages, in: 47th AIAA Aerospace Sciences Meeting including The New Horizons Forum and Aerospace Exposition, Aerospace Sciences Meetings, 2009. doi:10.2514/6.2009-737.

[26] H. J. Davis, H. D. Curchack, Shock Tube Techniques and Instrumentation, Tech. Rep. TR-1429, Harry Diamond Laboratories (1969).

[27] J. A. Fay, N. H. Kemp, Theory of Heat Transfer to a Shock-Tube End-Wall from an Ionized Monatomic Gas, Journal of Fluid Mechanics 21 (4) (1965) 659–672. doi:10.1017/s002211206500040x.

[28] OMEGA Engineering, Physical Properties of Thermoelement Materials.
URL https://www.omega.com/temperature/z/pdf/z021-032.pdf

[29] B. J. C. Birch, Characterisation of the USQ Hypersonic Facility Freestream, Ph.D. thesis, The University of Southern Queensland (2019).

[30] F. M. White, Viscous Fluid Flow, McGraw-Hill Education, 2005.

[31] R. East, A. Qasrawi, A Long Stroke Isentropic Free Piston Hypersonic Wind Tunnel, Tech. rep., Aeronautical Research Council, Reports and Memoranda, R & M No. 3844 (1978).

[32] D. R. Buttsworth, P. A. Jacobs, Measurement of Fluctuations in a Mach 4 Shock Tunnel Nozzle Flow, in: Proceedings of 7th Australasian Heat & Mass Transfer Conference, 2000, pp. 53–59.

[33] M. R. Fulghum, Turbulence Measurements in High-Speed Wind Tunnels Using Focused Laser Differential Interferometry, Ph.D. thesis, Pennsylvania State University (2014).

[34] L. Duan, M. M. Choudhari, A. Chou, F. Munoz, R. Radespiel, T. Schilden, W. Schröder, E. C. Marineau, K. M. Casper, R. S. Chaudhry, G. V. Candler, K. A. Gray, S. P. Schneider, Characterization of Freestream Disturbances in Conventional Hypersonic Wind Tunnels, Journal of Spacecraft and Rockets 56 (2) (2019) 357–368. doi:10.2514/1.a34290.